Australian Journal of Earth Sciences

ISSN: 0812-0099 (Print) 1440-0952 (Online) Journal homepage: https://www.tandfonline.com/loi/taje20

Magnetic petrophysical results from the Hamersley Basin and their implications for interpretation of magnetic surveys

W. W. Guo , Z-X Li & M. C. Dentith

To cite this article: W. W. Guo , Z-X Li & M. C. Dentith (2011) Magnetic petrophysical results from the Hamersley Basin and their implications for interpretation of magnetic surveys, Australian Journal of Earth Sciences, 58:4, 317-333, DOI: 10.1080/08120099.2011.552984

To link to this article: https://doi.org/10.1080/08120099.2011.552984

Published online: 27 May 2011.

Australian Journal of Earth Sciences (2011) **58**, (317–333)

Magnetic petrophysical results from the Hamersley Basin and their implications for interpretation of magnetic surveys

W. W. GUO[1]*, Z-X. LI[2] AND M. C. DENTITH[3]

[1]*School of Information and Communication Technology, Central Queensland University, Rockhampton QLD 4702, Australia.*
[2]*The Institute for Geoscience Research (TIGeR), Department of Applied Geology, Curtin University, GPO Box U1987, Perth WA 6845, Australia.*
[3]*Centre for Exploration Targeting, School of Earth and Environment, The University of Western Australia, 35 Stirling Highway, Crawley WA 6009, Australia.*

An extensive magnetic petrophysical investigation was carried out in the Hamersley Basin in Western Australia; which hosts large high-grade iron-ore deposits derived from banded iron formations (BIFs). Based on our new results, as well as those from previous studies, we demonstrate that the bulk susceptibility of BIF units has a bimodal distribution caused by the presence of chert-rich and magnetite-rich bands. The mean bulk susceptibility (MBS) of magnetite-rich bands is more than 10 times higher than that of chert-rich bands. Measurements of anisotropy of magnetic susceptibility (AMS) in BIF units show this to vary between 1.06 and 2.76. The natural remanent magnetisation (NRM) carried by iron ores varies with different deposits, and even within individual deposits. NRM measurements on non-ore units defined a northwesterly upward regional magnetic overprint (310°/–27°) present in the Fortescue and Hamersley Groups, and also in the lower Wyloo Group. Modelling of aeromagnetic data over the Hamersley Range demonstrates that the effects of AMS and NRM are significant and must be accounted for. The effects of AMS and NRM on magnetic anomalies due to BIFs depend on the volume fraction of magnetite-rich members in a BIF unit. Forward modelling of magnetic and gravity responses, using petrophysical results summarised in this study, over a mined hematite ore deposit in Tom Price indicates that TMI variations are expected to be significantly reduced in areas of mineralisation. However, magnetic data alone are not a reliable indicator of the presence of mineralisation because of other causes of reduced magnetism in BIFs.

KEY WORDS: Magnetic petrophysics, NRM, AMS, Magnetic modelling, Banded iron formation, Hematite ore, Hamersley Basin

INTRODUCTION

The Hamersley Basin, located in the Pilbara Block in northwestern Western Australia, is about 500 km long and 250 km wide, with a west-north-westerly elongation (Trendall 1983) (Figure 1). The basin is defined by the extent of the Hamersley Group sedimentary and volcanic rocks and contains extensive banded iron formations (BIFs) and large hematite-goethite iron deposits, which occur with the BIF units.

BIFs usually produce strong magnetic anomalies, enabling the prospective stratigraphy to be readily mapped. For this reason, magnetics has been extensively used in iron ore exploration (Webb 1966; Seguin 1971; Kerr *et al.* 1994; Butt & Flis 1997). Understanding magnetic responses for exploration at a prospect scale is much more difficult because the magnetic properties of both BIF and iron ores are complex. It has long been recognised that, in general, iron ores are less magnetic than the BIFs, but confident interpretation of magnetic data requires a good understanding of the magnetic properties of the different lithological units in the area of interest.

In the Hamersley Basin, several studies related to magnetic petrophysics were conducted before this study. These include Porath & Chamalaun (1968), Chamalaun & Dempsey (1978), Embleton *et al.* (1979), Clark & Schmidt (1986, 1994), and Li *et al.* (1993), but these studies were limited both geographically and stratigraphically. Between 1995 and 1999, incorporating a paleomagnetic study sponsored by MERIWA and three industry partners on the genesis of the Hamersley iron ores (Li *et al.* 2000), a systematic magnetic petrophysical study was carried out in the Hamersley Basin as a part of a PhD project (Guo 1999). A total of 568 oriented block samples and 26 industrial drill cores were collected. These samples cover most of the geological units in the region. More than 1000 specimens were prepared from these samples, from which over 1000 measurements of magnetic susceptibility/anisotropy and remanent

*Corresponding author: w.guo@cqu.edu.au

ISSN 0812-0099 print/ISSN 1440-0952 online
DOI: 10.1080/08120099.2011.552984

magnetisation were made. In this paper, we first present these magnetic petrophysical results and then discuss their implications for the interpretation of magnetic data from the Hamersley Basin.

GEOLOGICAL BACKGROUND

Archean (>2800 Ma) granite-greenstone outcrops over most of the northern half of the Pilbara Block and is unconformably overlain by the Hamersley Basin in the southern half of the block except for a few exposures in inliers or domes within the basin (Figure 1). Within the basin there are three major stratigraphic units, ranging in age from Late Archean to Early Proterozoic (2780–2200 Ma). These are the Fortescue, Hamersley and Turee Creek Groups (Figure 2), which are collectively referred to as the Mount Bruce Supergroup. Hamersley Basin rocks are unconformably overlain to the south by the 2200–1800 Ma rocks of the Ashburton Basin. Rocks of the Hamersley and Ashburton Basins have been subjected to greenschist facies metamorphism during the *ca* 2200 Ma Ophthalmian Orogeny and/or the *ca* 1800 Ma Capricorn Orogeny (Cawood & Tyler 2004).

The Fortescue Group is the lowermost stratigraphic unit of the Hamersley Basin dated at 2780–2629 Ma (Trendall *et al*. 2004) and rests unconformably on an Archean granite-greenstone basement. The Fortescue Group is up to 1.8 km thick and consists of low-grade volcanic and sedimentary rocks.

The Hamersley Group conformably overlies the Fortescue Group and is conformably overlain by the Turee Creek Group. It is approximately 2.5 km thick and consists of four important iron formations separated by sequences of dolomites, shales and volcanics. The Hamersley Group is divided, in ascending order, into the following eight formations: the Marra Mamba Iron Formation, the Wittenoom Dolomite, the Mount Sylvia Formation, the Mount McRae Shale, the Brockman Iron Formation, the Weeli Wolli Formation, the

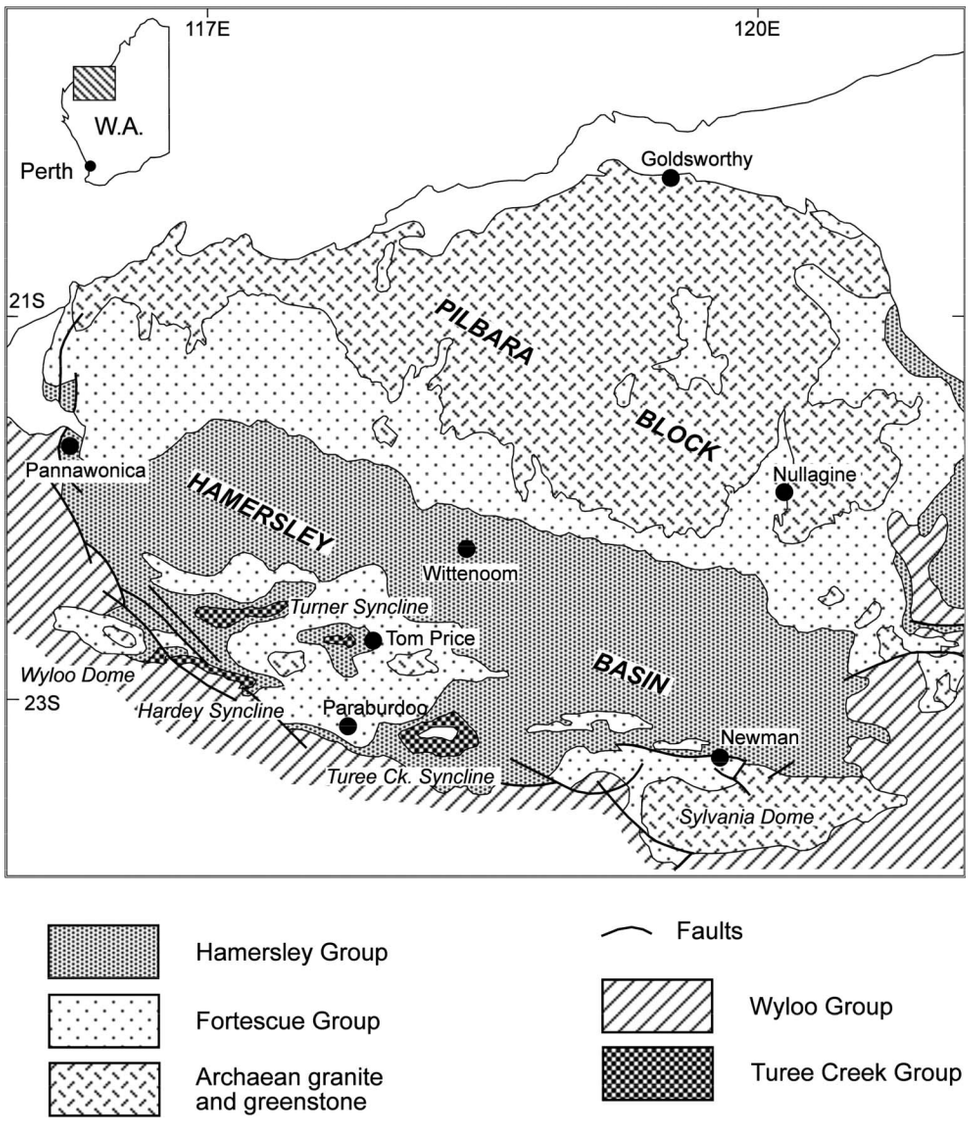

Figure 1 Simplified geological map of the Hamersley Basin (after Trendall 1983).

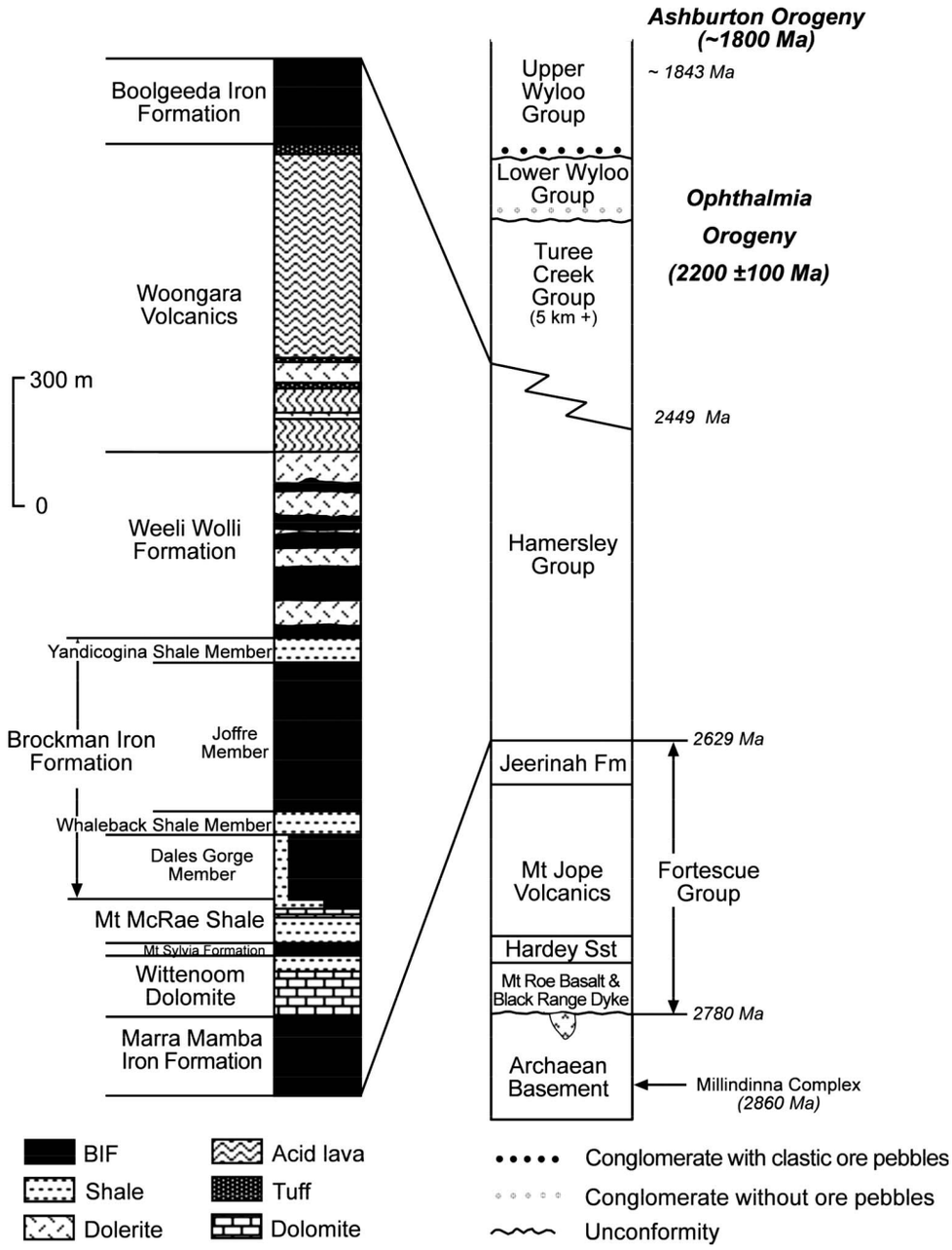

Figure 2 Stratigraphical ideal column of the Hamersley Basin.

Woongarra Volcanics, and the Boolgeeda Iron Formation (Figure 2). Most of the iron ore deposits occur in the Brockman Iron Formation, approximately 620 m thick, and the Marra Mamba Iron Formation, approximately 230 m thick, although both the Weeli Wolli Formation and the Boolgeeda Iron Formation also contain minor enrichments. The Brockman Iron Formation consists of four members: the Dales Gorge, Whaleback Shale, Joffre, and Yandicoogina Shale Members (Figure 2). The age span of the Hamersley Group is well constrained to between 2629 Ma and 2449 Ma (Trendall *et al.* 2004).

The Turee Creek Group comprises fine- to coarse-grained siliclastic rocks with local occurrences of chemical sediments. The Wyloo Group, formed after the *ca* 2200 Ma Ophthalmian Orogeny, unconformably overlies the Mount Bruce Supergroup (i.e., the Fortescue, Hamersley and Turee Creek Groups). It has a maximum thickness of approximately 10–12 km, and is subdivided, in ascending order, into: the Beasley River Quartzite, the Cheela Springs Basalt, the Mount McGrath Formation, the Duck Creek Dolomite, and the Ashburton Formation. The Wyloo Group and older rocks were deformed by the *ca* 1800 Ma Capricorn Orogeny (Cawood & Tyler 2004).

For more details about the geology and classification of iron ores in the Hamersley Basin, we refer readers to Trendall (1983), Kneeshaw (1984), Morris (1985) and Harmsworth *et al.* (1990). For recent updates on regional tectonostratigraphic correlations and precise age

constraints, we refer readers to Cawood & Tyler (2004) and Trendall *et al.* (2004).

SAMPLING AND DATA ACQUISITION

Sampling and specimen preparation

The stratigraphic distribution of the 568 block samples comprising this study is listed in Table 1. The localities of individual sampling sites are given in Guo (1999) and Li *et al.* (2000). Most sampling sites were located at road-cuts, creek beds and open pits so as to minimise the effects of lightning and/or weathering. In addition, 26 non-oriented industrial core segments were also collected for rock-magnetic analyses.

Oriented block samples were drilled with a 25 mm diameter table drill in the Paleomagnetism Laboratory at The University of Western Australia (UWA). Each core sample was divided into one or more standard paleomagnetic specimens of 22 mm height. Industrial drill-core samples were re-cored parallel to the long axis of the sample. A total of over 1000 specimens were obtained.

Magnetic susceptibility and anisotropy measurements

Low-field magnetic susceptibility and anisotropy of every specimen were measured in the Paleomagnetic Laboratory at UWA using a Bartington MS2 susceptibility system. The bulk susceptibility and anisotropy of a specimen were calculated using the measured three principal components of magnetic susceptibility.

Remanent magnetisation measurement

Natural remanent magnetisation (NRM) is defined as the remanent magnetisation present in a rock sample prior to laboratory treatment (Butler 1992). In this study, NRM orientation in the current geographic coordinates is referred to as the *in situ* NRM. NRM depends on direction and intensity of the paleo- and/or current geomagnetic field, geological processes during and after rock formation, and the post-formation tectonic history of the rock. Typically, NRM is composed of a primary and one or more secondary remanent magnetisms (RMs). The primary RM represents the magnetism acquired during rock formation. Secondary RMs can result from chemical changes in ferromagnetic minerals (which may be diagenetic or metamorphic in origin), exposure to nearby lightning strikes, or long-term exposure to the geomagnetic field (Butler 1992). In some paleomagnetic studies, secondary RMs are regarded as noise. However, regionally extensive secondary RMs may be important for understanding magnetic responses because it is the NRM (primary + secondary RMs), rather than the individual RM components, which, together with induced magnetisation, produce magnetic anomalies. If the intensity and/or direction of a strong RM varies across the area of interest so too will the NRM and hence the magnetic response from a particular unit. In particular, its spatial relationship to bedding attitude can also be important. Pre-folding remanent magnetism is acquired before a deformation and has a constant orientation relative to the bedding plane. Post-folding remanent magnetism is acquired after a deformation and its orientation varies relative to the bedding plane. Significantly, whether an intense RM is pre-folding or post-folding can result in different magnetic responses from the same geological scenario (Clark & Schmidt 1986, 1994).

A 2G Enterprises 755 cryogenic magnetometer was used to measure remanent magnetisation. Both orientation and magnitude of remanent magnetisation were measured. Stepwise thermal or alternating field (AF) demagnetisation was applied to most specimens to isolate the component RMs. Detailed analysis and interpretation of these data can be found in Li *et al.* (2000).

METHODOLOGY OF DATA STATISTICS

Conventional scalar statistics were applied to the analysis of non-directional data, such as bulk susceptibility and amplitude of anisotropy of magnetic susceptibility (AMS).

Table 1 List of oriented samples and their stratigraphic distribution.

Group	Formation/type	Site number	Samples	Lithology
Wyloo	Duck Creek Dolomite	2	10	Dolomite, sandstone
	Mount McGrath Fm	1	6	Hematite conglomerate
	Cheela Spring Basalt	2	9	Basalt
Turee Creek		2	17	Dolomite
Hamersley	Boolgeeda IF	6	38	BIF, siltstone
	Woongarra Volcanics	3	18	Rhyolite
	Weeli Wolli Fm	6	27	BIF
	Brockman IF	46	205	BIF, iron ore
	Mount McRae Shale	1	9	Shale, dolomite
	Mount Sylvia Fm	8	28	BIF
	Wittenoom Dolomite	13	76	Dolomite
	Marra Mamba IF	11	50	BIF, chert, iron ore
Fortescue		11	69	Basalt, pillow lava
	Dyke	2	6	Dolerite

NRM is a vector so both its intensity and orientation are important for understanding magnetic responses. Fisher statistics are widely used in directional data analysis (Tarling 1983; Butler 1992). Fisher statistics suppose that each element has equal weight or unit intensity, in spite of the differences in real intensity, and all directions are expected to be distributed according to the 'spherical normal' or Fisher distribution. Obviously the Fisher method cannot provide information on NRM intensity.

General and directional vector analyses

In this study, we use two approaches for NRM vector analysis, referred to as general vector analysis (GVA) and directional vector analysis (DVA). In GVA, each measurement is weighted by its intensity. The mean vector is defined in terms of its declination (D) with respect to north, inclination (I) with respect to horizontal, and intensity (J_r); with angular deviation λ as a measure to assess the precision of the mean and hence the degree of scatter of a set of NRM vectors.

DVA is modified from Fisher analysis so as to be comparable with GVA. In DVA, each NRM is regarded as a unit vector. Its outcome includes a mean declination (D) and inclination (I), with angular deviation δ used to represent the precision of the mean. The mean direction from DVA is exactly the same as the Fisher mean. However, it should be noted that DVA is generally applicable to any directional datasets, but theoretically, Fisher analysis is for datasets with a spherical normal distribution only.

GVA and DVA normally give somewhat different mean directions for the same data set, but the difference should be small if the studied geological unit is magnetically homogeneous. A detailed description of GVA and DVA is given in Appendix 1.

Strategy for NRM data processing

NRM data from BIF sites with little likelihood of lightning-strike effects were first analysed using GVA to see if any concentrated NRM direction could be found. DVA and fold test (determination of the age of magnetism relative to a folding event, see Appendix 2), wherever available, were then used to assess the significance of such NRM concentrations, and to define its temporal relationship to deformation at the site. NRM data of iron ores collected from open pits are unlikely to be affected by lightning, so GVA was automatically applied to such data.

Since the NRM intensity of non-BIF units is usually very low, the NRM orientation for non-BIF samples is more significant than the intensity information for magnetic modelling. This is because AMS and self-demagnetisation of non-BIF rocks would not be expected to affect their NRM, so NRM directions carried by non-BIF rocks may be very useful in identifying any regional magnetic overprint that may be significant for magnetic modelling. DVA was used for analysing NRM data for each non-BIF site. We selected one specimen from each sample for complete demagnetisation. Data obtained from such paleomagnetic cleaning were used as a reference to identify any magnetism acquired due to surface weathering or transportation.

MAGNETIC PETROPHYSICAL RESULTS

Bulk magnetic susceptibility

The four major BIF formations in the Hamersley Group exhibit a logarithmic bimodal distribution in bulk susceptibility (Figure 3). The mean bulk susceptibility (MBS) of these units is listed in Table 2.

The chert-rich and/or hematised samples from BIF units carry only weak magnetism whereas those containing more magnetite have stronger magnetism as indicated by MBS greater than 3500×10^{-5} SI, which

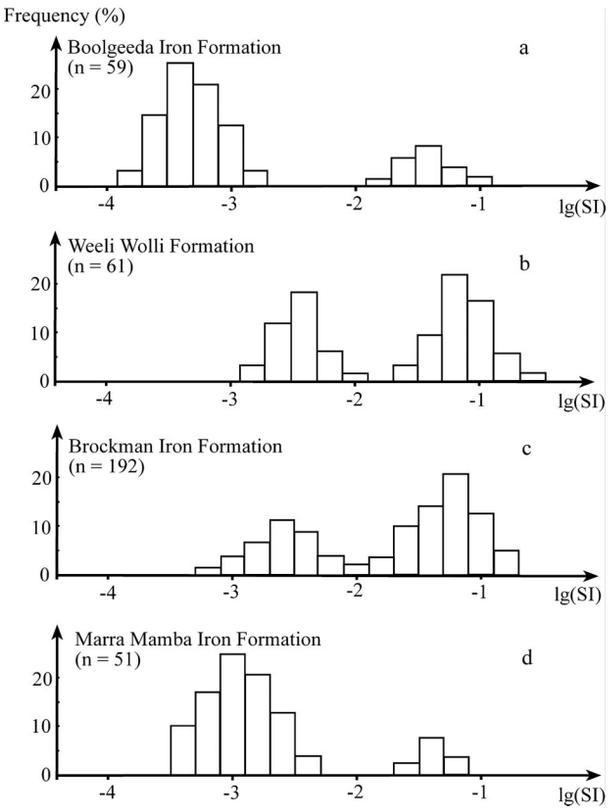

Figure 3 Histograms of mean bulk susceptibility (MBS) of BIFs.

Table 2 Mean bulk susceptibility (MBS) of the Hamersley Group BIFs.

BIF Unit	Population 1 ($\times 10^{-5}$ SI)			Population 2 ($\times 10^{-5}$ SI)		
	n	MBS	SD	***n***	MBS	SD
Boolgeeda IF	47	36	42	12	3635	4535
Weeli Wolli Fm	25	352	214	36	5361	2849
Brockman IF	74	319	230	118	4225	2866
Marra Mamba IF	44	103	87	7	4970	1638

n, number of specimen; SD, standard deviation.

is at least ten times stronger than that of the chert-rich and/or hematised samples. This clearly demonstrates that great variation exits in MBS within individual BIF units, and the measured value will depend on the lithological make up of the unit where a sample was collected.

Both hematite and hematite-goethite ores exhibit a logarithmic normal distribution and have comparable values of MBS (Table 3). Compared with both of these ore types, the MBS of the Barrett-Lennard hematite conglomerate ore in the Mount McGrath Formation is lower and better grouped.

All other non-BIF rocks are characterised by low MBS of $<100 \times 10^{-5}$ SI (Table 3), but dolerite dykes have a moderate MBS that can produce significant linear magnetic features in non-BIF geological terrains.

Anisotropy of magnetic susceptibility of BIF units

Our study shows that most BIF units have a well-developed magnetic foliation parallel or sub-parallel to bedding (Figure 4). The average anisotropy of these BIF units is given in Table 4. Brockman BIFs are the most anisotropic in magnetic susceptibility with an average AMS of $\sim$1.3, the maximum being up to 2.8. Weeli Wolli BIFs are also anisotropic but Marra Mamba BIFs are almost isotropic. Clark & Schmidt (1986, 1994) reported that the AMS can be up to 4.0 for fresh BIFs in the Hamersley Basin.

Natural remanent magnetisation

BIF UNITS

GVA was applied to NRM data from 14 BIF sites that showed little evidence of lightning effects, and the results are listed in Table 5. Unfortunately, none of these sites shows any NRM concentration. Since a few intense NRM vectors in a site may dominate the vector mean, it is necessary to make a further NRM orientation analysis to see if any concentrated NRM directions can be found at these sites. DVA analysis reveals that four sites (BI02, BI03, BI04, and BM05) have concentrated NRM directions (Table 6). These four sites give a well concentrated *in situ* NRM direction that is northwesterly upward (339°/–26°), although the majority of BIF sites have scattered NRM directions.

Four samples comprising orientated BIF drillcores described by Clark & Schmidt (1986) also revealed a northwesterly upward NRM direction. However, the average intensity of 45.5 ± 18.6 A/m is much greater than that of our vector means for BIF sites.

IRON ORES

The six sites comprising hematite ores from the Mt Whaleback deposit give a well or marginally concentrated NRM mean (Table 7). The NRM mean direction of four sites (NM03, NM07–09) is northwesterly whereas the direction of the other two sites (NM01 and NM04) is southwesterly. However, they all have downward inclination, between 45° and 51°. The average NRM intensity varies from 641 to 1130 mA/m. Detailed analysis of paleomagnetically cleaned data revealed a late-Ophthalmian magnetic overprint direction of $D = 248.8°$ and $I = 57.8°$ from the Mt Whaleback deposit (Li *et al.* 2000).

Among the six sites comprising hematite ores from the Tom Price mine, sites TP03, TP04 and TP08 have well-defined NRM means (Table 7). Sites TP05 and TP06

Table 3 MBS of non-BIF units and iron ores in the Hamersley Basin.

Formation/dyke	*n*	MBS (10^{-5} SI)	SD (10^{-5} SI)
Duck Creek Dolomite	10	48	40
Mount McGrath hematite conglomerate ore	15	169	44
Cheela Springs Basalt	12	68	28
Turee Creek dolomite	24	22	4
Woongarra Volcanics	32	39	20
Mount McRae Shale	21	62	32
Wittenoom Dolomite	139	21	16
Jeerinah Formation	25	50	8
Bunjinah Formation	24	54	7
Pyradie Formation	12	56	7
Boongal Formation	10	50	4
Maddina Basalt	14	52	22
Tumbiana Formation	34	68	30
Hematite ore (Brockman iron ore)	131	349	192
Hematite-goethite ore (Marra Mamba iron ore)	111	356	303
Dolerite dyke	18	623	612

n, number of specimen; SD, standard deviation.

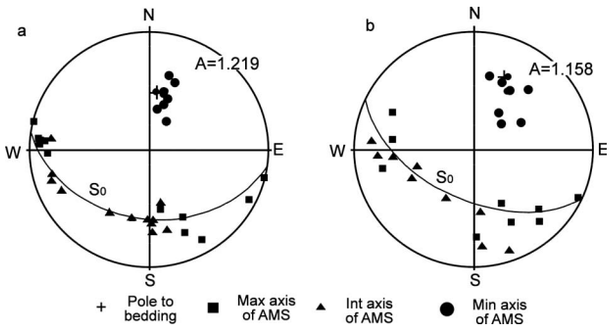

Figure 4 Anisotropy of magnetic susceptibility of BIFs. (a) Weeli Wolli BIF (WW06). (b) Brockman BIF (BM02). S_0 is the average bedding plane.

Table 4 Average AMS of BIF units in the Hamersley Group.

BIF Unit	Number of specimens	Mean AMS	Minimum AMS	Maximum AMS
Boolgeeda IF	71	1.10	1.07	1.14
Weeli Wolli Fm	61	1.24	1.06	1.88
Brockman IF	162	1.31	1.06	2.76
Marra Mamba IF	64	1.07	1.08	1.09

Table 5 GVA means of NRM of the BIF sites little affected by lightning.

BIF Unit	Site	*n*	G-Dec (°)	G-Inc (°)	λ (°)	J_r (mA/m)	S-Dec (°)	S-Inc (°)	λ (°)
Boolgeeda IF	BI02	9	344	−47	34	67	7	−4	44
	BI03	14	330	−39	36	2	351	−10	47
	BI04	13	356	−30	27	1620	285	−64	31
Weeli Wolli Fm	WW03	11	203	16	35	616	207	−9	28
	WW06	10	347	−27	27	2954	349	10	32
Brockman IF	JF01	11	13	27	32	356	10	9	33
	JF02	10	308	−22	47	147	315	−39	44
	JF03	9	229	43	26	735	61	−12	83
	JF04	15	187	51	63	294	197	−13	74
	DG04	19	283	7	51	298	5	−18	70
	BM04	10	251	−19	62	4502	248	−14	62
	BM05	9	345	−3	37	1473	345	−7	37
	BM06	8	261	−33	53	32 612	275	−37	53
Marra Mamba IF	MM04	12	244	53	58	95	232	19	57

n, number of specimen; λ, angular deviation; J_r, intensity of NRM; G-D/G-Inc, declination/inclination in the current geographic coordinates; S-Dec/S-Inc, declination/inclination after restoring the bedding plane to the horizontal.

Table 6 DVA means of NRM of the BIF sites without effect of lightning strike.

BIF Unit	Site	*n*	G-Dec (°)	G-Inc (°)	δ (°)	S-Dec (°)	S-Inc (°)	δ (°)
Boolgeeda IF	BI02	9	340	−45	22	3	−4	22
	BI03	14	321	−35	16	343	−12	16
	BI04	13	344	−27	22	287	−53	22
Brockman IF	BM05	9	347	−11	20	348	−15	20

n, number of specimen; δ, angular deviation; G-D/G-Inc, declination/inclination in the current geographic coordinates; S-Dec/S-Inc, declination/inclination after restoring the bedding plane to the horizontal.

Table 7 GVA means of *in situ* NRM of some iron-ore sites.

Deposit	Site	*n*	G-Dec (°)	G-Inc (°)	λ (°)	J_r (mA/m)
Barrett-Lennard	MG01	15	310	−15	16	417
Channar	CM02	6	306	−11	29	600
Paraburdoo	PD02	9	287	9	24	1186
Tom Price	TP03	12	1	11	17	218
	TP04	7	338	4	19	496
	TP05	4	312	−5	25	390
	TP06	4	336	23	27	1847
	TP07	6	334	−55	41	596
	TP08	2	29	42	4	1569
Whaleback	NM01	11	261	45	23	893
	NM03	16	297	50	20	853
	NM04	7	236	51	10	830
	NM07	8	310	47	15	1130
	NM08	8	333	45	32	708
	NM09	17	298	51	29	641

n, number of specimen; λ, angular deviation; J_r, intensity of NRM; G-D/G-Inc, declination/inclination in the current geographic coordinates.

have marginally concentrated NRM, but the NRM at site TP07 is scattered. Site TP03 has an average NRM orientation directed sub-horizontally northwards (001°/11°) whereas site TP08 is downwards northeast. The mean NRM direction of the other four sites is toward the northwest, but two (TP04 and TP06) are downward and the other two (TP05 and TP07) are upward. The average NRM intensity of the five individual sites varies from 218 to 1847 mA/m.

Only one site was sampled in each of the Channar, Paraburdoo, and Barrett-Lennard deposits. Each site gives a well or marginally concentrated NRM mean that is northwesterly upward (Table 7). The mean NRM intensity varies from 417 mA/m to 1186 mA/m.

NON-BIF UNITS

Of the total 33 sites, concentrated NRM is found in 20 sites (Table 8). It is interesting to note that 17 sites among the 20 concentrated sites have northwesterly upward NRM directions. The remaining three sites (DD01, WG03 and BJ02) each have a concentrated NRM direction too (Table 8), but the mean directions are inconsistent with each other.

REGIONAL MAGNETIC OVERPRINT

There seems to be a regional magnetic overprint directed moderately upwards to the northwest in many non-BIF units in the Hamersley Basin (Table 8; for details see Li *et al.* 2000). A similar direction was also revealed by previous studies on volcanic rocks of the Fortescue Group (Schmidt & Embleton 1985; Li *et al.* 1993), the Wittenoom Dolomite (Li *et al.* 1993), and fresh dolerite dykes and BIFs (Clark & Schmidt 1986) (Table 9).

When DVA is applied to all of the 25 sites that share this general direction, a well-grouped, northwest upwards remanence direction (310°/−27°) is defined. This direction is considered to be the regional magnetic overprint throughout the Hamersley and Fortescue Groups, and may extend in to the lower Wyloo Group because it also appears in the Cheela

Springs Basalt and the Mount McGrath Formation. The overlying Duck Creek Dolomite has a different NRM direction (Table 8).

MAGNETIC MODELLING

When quantitative modelling of observed responses is required for detailed magnetic interpretation, particularly involving highly magnetised geological units, the influence of AMS, NRM, and/or self-demagnetisation must be considered. Otherwise, significant errors will result due to miscalculation of modelled anomaly amplitudes and also lateral displacement of responses. Readers are referred to Appendix 2 for details of these effects in magnetic modelling.

Table 8 Site-mean NRM directions of non-BIF units.

Group/Dyke	Formation	Site	*n*	G-Dec (°)	G-Inc (°)	δ (°)
Wyloo	Duck Creek Dolomite	DD01	4	105	−61	10
	Mt McGrath Fm	MG01	15	312	−15	14
	Cheela Springs Basalt	CB01	6	296	−25	13
Hamersley	Wongarra Volcanics	WG01	6	302	−26	13
		WG02	6	316	−34	20
		WG03	8	254	−68	16
	Wittenoom Dolomite	WD02	6	304	−26	7
		WD03	6	311	−30	7
		WD04	9	307	−21	11
		WD07	6	326	−31	17
		WD08	3	315	−45	6
		WD10	7	315	−30	5
		WD11	5	314	−30	12
		WD12	7	300	−11	4
Fortescue	Jeerinah Fm	JR02	8	322	−23	19
	Bunjinah Fm	BJ01	8	312	−29	14
		BJ02	6	338	58	21
	Maddina Basalt	KS01	6	322	−46	18
		MB01	4	306	−13	4
Dyke		RD01	4	334	−19	21

n, number of sample/specimen; δ, angular deviation; G-D/G-Inc, declination/inclination in the current geographic coordinates.

Table 9 NRM data of previous studies and the DVA mean of the regional overprint.

Geological unit	G-Dec (°)	G-Inc (°)	*d* (°)	Reference
Dolerite (DDH 44)	300	−47	–	Clark & Schmidt (1986)
Weeli Wolli BIF (DDH 44)	306	−38	–	Clark & Schmidt (1986)
Joffre BIF (DDH 44)	284	−26	–	Clark & Schmidt (1986)
Dales Gorge BIF (ND93/80)	283	−17	–	Clark & Schmidt (1986)
Dales Gorge BIF (DDH 42)	294	−20	–	Clark & Schmidt (1986)
Wittenoom Dolomite	305	−35	–	Li *et al.* (1993)
Jeerinah basalt	310	−23	–	Li *et al.* (1993)
Mt Jope Volcanics	304	−19	–	Schmidt & Embleton (1985)
DVA mean (25 sites)	310	−27	13	This study

Modelling of aeromagnetic data from the Hamersley Range

AEROMAGNETIC SIGNATURES

Figure 5 shows the enhanced TMI data from the central part of the Hamersley Range in the northern Hamersley Basin. When compared with the geological map in the region (Figure 6, Thorne *et al.* 1996), the magnetic highs correlate well with the extensive exposures of the Brockman Iron Formation, whereas the magnetic lows are usually correlated with Cainozoic alluvium and colluvium in the central area and creeks. As expected, the outcrops of the Wittenoom Dolomite, the Mount McRae Shale and the Mount Sylvia Formations together correlate with magnetic lows and/or flat magnetic fields. The Marra Mamba Iron Formation crops out only in the southernmost Hamersley Range, which lies outside the modelling area, but it may extend northwards beneath cover rocks. Since the strata along the Hamersley Range are generally flat-lying, the underlying Marra Mamba Iron Formation is also likely to have low bedding dip angles (Thorne *et al.* 1996). Thus, it mainly contributes a regional background field to the TMI and has little effect on the local magnetic anomalies.

MAGNETIC MODELLING

A NNE-trending profile crossing the Hamersley Range (Figure 5) was chosen for 2D magnetic modelling. The

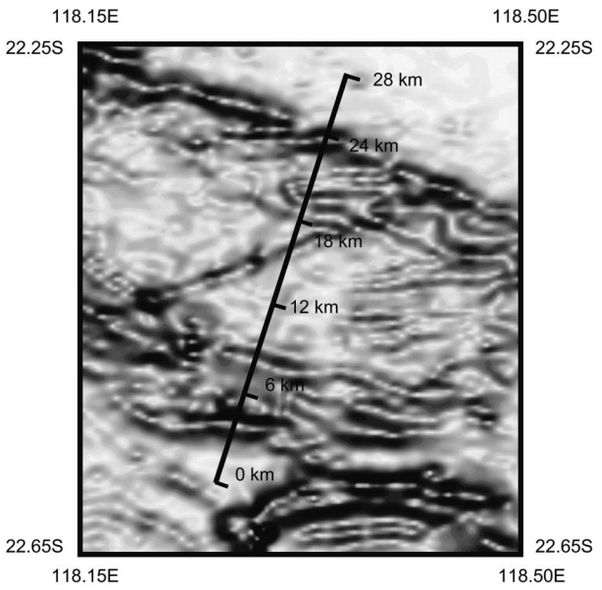

Figure 5 TMI image of the Hamersley Range. Profile for magnetic modelling is shown as a NNE line.

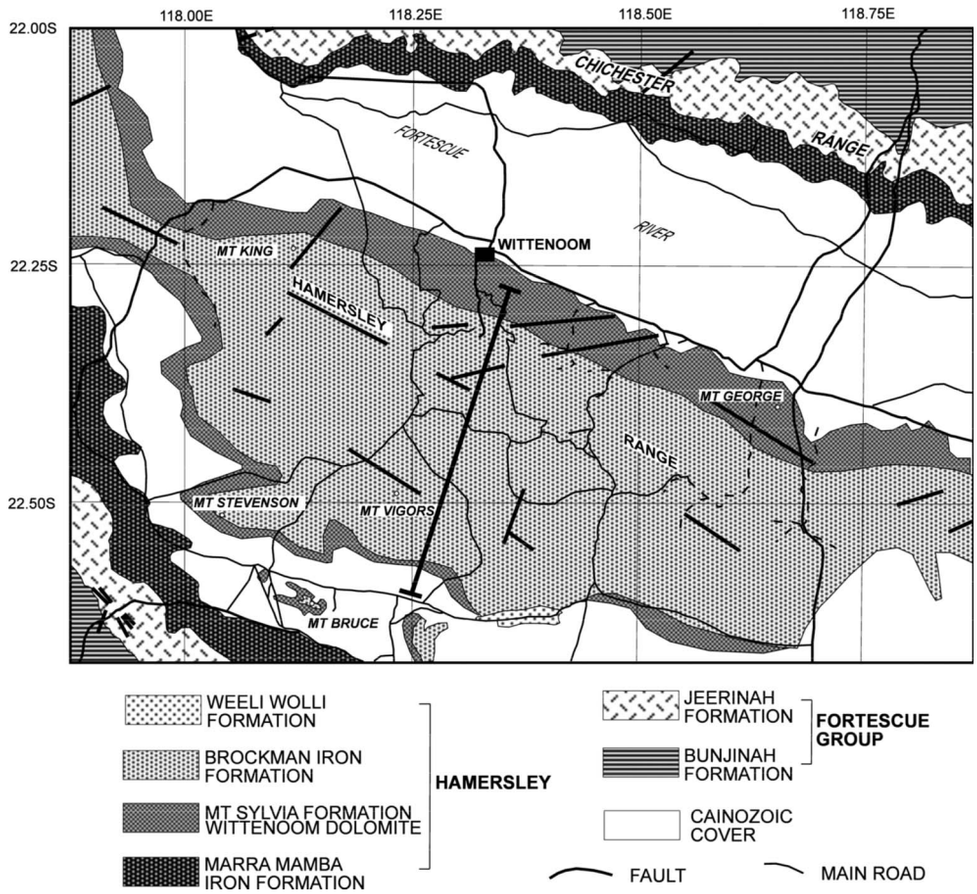

Figure 6 Simplified geological map of the Hamersley–Chichester Range region (after Thorne *et al.* 1996). The NNE tending thicker line indicates the aeromagnetic modelling profile.

ground surface topography, though relatively flat in this area, and the flight fluctuation during the aeromagnetic survey may have contributes some local and/or random variations to the magnetic data. Therefore, the data set was first smoothed so as to suppress both short wavelength and random variations originated from these factors. A mean value of 5240 nT was determined from whole dataset statistics along the profile as a background field. The residual data set is then obtained by subtracting this background field from the smoothed data. The residual magnetic profile is used as the observed data in our magnetic modelling (Figure 7).

Geological constraints on the model are mainly provided by the local geological map (Thorne *et al.* 1996). Magnetic properties of individual entities are based on the results summarised in this study. The overall magnetism of the Mount McRae Shale and the Mount Sylvia and Wittenoom Dolomite, sitting between the overlying Brockman Iron Formation and the underlying Marra Mamba Iron Formation, is generally very low, although there are a few thin highly magnetic layers within these units. Consequently, these three formations can be regarded as one combined unit, and are less important in the magnetic modelling in this specific circumstance. The major magnetic source contributing to the residual magnetic field variation is likely to be the overlying Brockman Iron Formation, with minor contributions from the underlying Marra Mamba Iron Formation.

Given the regional scale of the modelling, the Brockman Iron Formation is considered as a whole rather than being separated into component members. An average bulk susceptibility of 0.45 SI is assumed for the BIF members. The shale members occupy about 20% of the whole volume of this formation, along with some fraction of 'shale bands' in BIF members (Thorne & Tyler 1997). Based on this volume fraction and magnetic properties obtained by Clark & Schmidt (1986, 1994) and Guo (1999), an average bulk susceptibility of 0.3 SI, i.e. two-thirds of the assumed average bulk susceptibility for the BIF members, is estimated for the whole formation. Using an average AMS of 1.7 for BIFs after taking the volume fraction into account, vertical and horizontal susceptibility components of 0.205 SI and 0.348 SI, respectively, can be calculated for the flat-lying BIF sections. Following a similar process, an *in situ* NRM of 30 A/m directed upwards to the northwest (310°/–27°) was used for the Brockman Iron Formation.

The underlying Marra Mamba Iron Formation is assumed to be fresh. Since BIF members occupy only about 20% of the whole volume of this formation (Harmsworth *et al.* 1990; Thorne & Tyler 1997), the

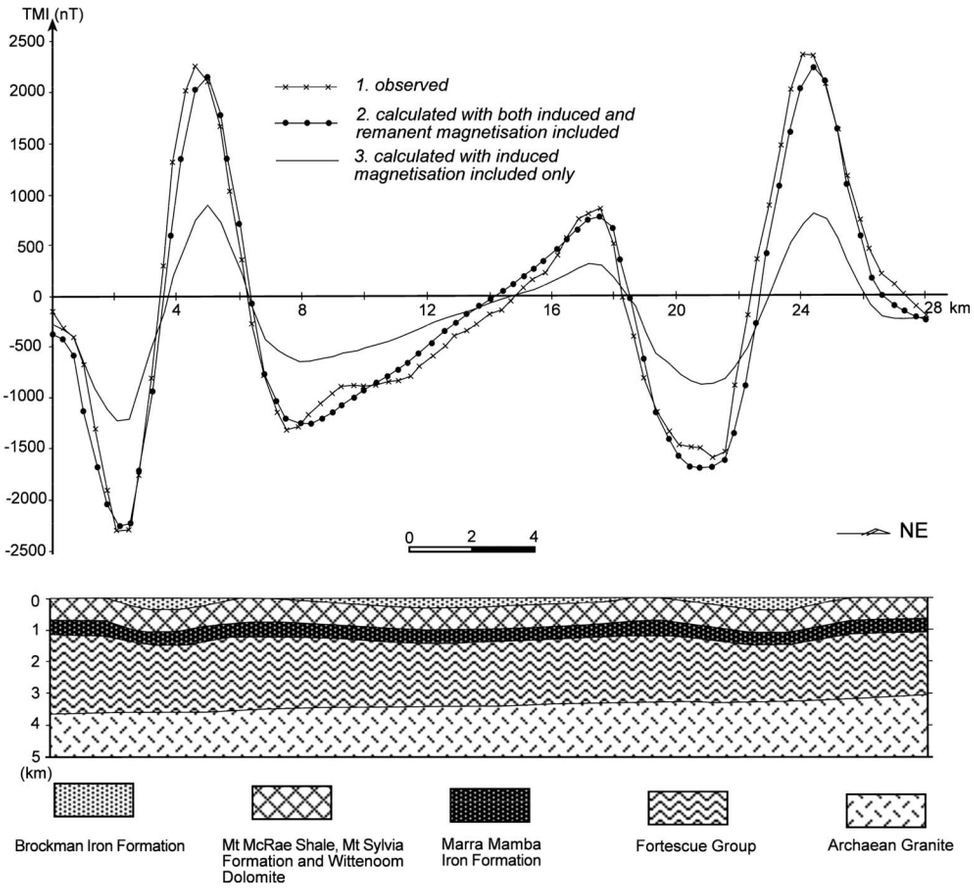

Figure 7 Magnetic modelling profile over the Hamersley Range. Magnetic properties used are listed in Table 10.

average bulk susceptibility and NRM of this formation are estimated to be about 0.1 SI and 10 A/m, respectively. The magnetic properties of all the units and other parameters used in the modelling are given in Table 10.

The preferred 2D model is shown in Figure 7. Generally, a good fit between the observed (curve 1) and modelled magnetic fields (curve 2) has been achieved. The minor differences in some local areas may be due to errors in the selection of magnetic properties and model simplifications. The modelling results suggest that the residual thickness of the Brockman Iron Formation varies laterally from a few meters to 400 m due to surface erosion. The modelling requires that the Mount McRae Shale comes to surface at around the 6 km mark in the profile (Figure 7), which is consistent with geological mapping (Thorne *et al*. 1996). The model also requires the Mount McRae Shale to be close to the surface at around the 20 km mark in the profile (Figure 7), although not actually outcropping.

The modelled magnetic response without considering the *in situ* NRM (curve 3) is significantly different from the observed residual field (curve 1) (Figure 7). This means that the NRM carried by BIF units cannot be ignored in magnetic modelling over BIF-involved areas. The good fit between the observed and calculated magnetic fields (curves 1 and 2) suggests that the northwesterly upward NRM (310°/–27°) is broadly correct and can be used in regional magnetic modelling in the Hamersley Basin. This modelling also shows that when selecting the magnetic properties for a BIF unit as a whole, many factors, such as AMS, NRM, and the volume fraction of non-BIF members/bands within the BIF unit, should be taken into account.

Table 10 Magnetic properties of the geological units and other parameters used in the magnetic modelling in the Hamersley Range.

Geological unit	Induced magnetism	NRM	EMF and remark
Brockman IF	$A = 1.7$	$J_r = 30$ A/m	$F_0 = 53\,800$ nT
	$k = 0.300$ SI	Dec $= 310°$	$I_0 = -55°$
	$k_x = 0.348$ SI	Inc $= -27°$	$D_0 = 1°$
	$k_z = 0.205$ SI		
Marra Mamba IF	$A = 1.4$	$J_r = 10$ A/m	Flight height = 150 m
	$k = 0.100$ SI	Dec $= 310°$	Profile direction: N16°E
	$k_x = 0.111$ SI	Inc $= -27°$	Strike of models: 286°
	$k_z = 0.079$ SI		
Other units	$A = 1.0$	$J_r = 1.0$ A/m	
	$k = 0.01$ SI	Dec $= 310°$	
		Inc $= -27°$	

Magnetic and gravity responses of a high-grade hematite deposit

It has long been recognised that magnetic data can potentially be used for targeting in the Hamersley Basin, with mineralisation expected to be associated with subdued magnetic response compared with BIF dominated areas. However, as pointed out by Kerr *et al.* (1994) and Hawke & Flis (1997) care must be taken because phenomenon such as weathering can also result in subdued magnetic responses of BIFs. Gravity surveys provide a means of identifying false positives due to the high density of the ores.

With the improved database of magnetic petrophysical results and density data from the Hamersley Basin (Guo 1999; Guo & Howard 2000), it is interesting to

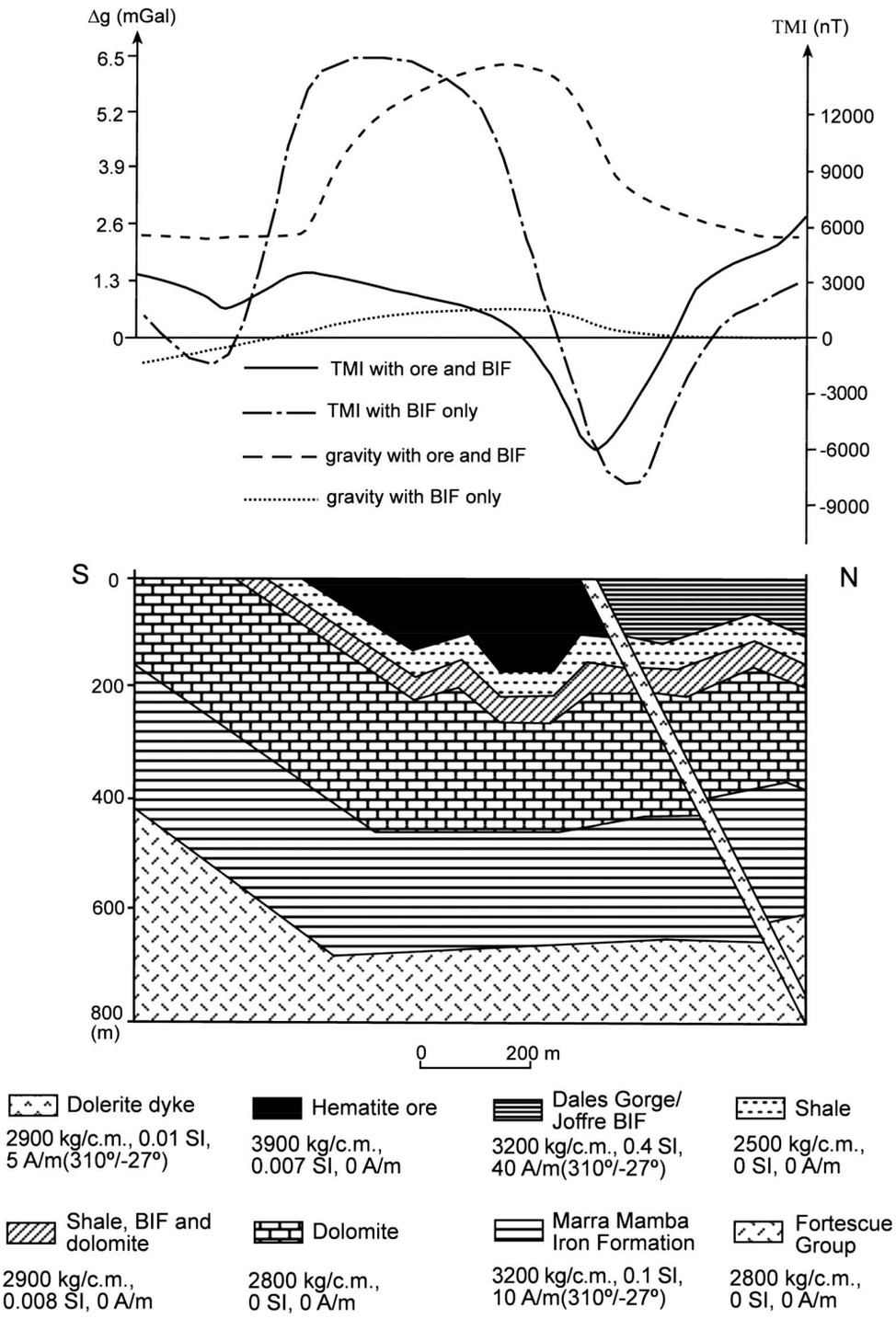

Figure 8 Simplified geological cross-section of the Section 6 deposit (modified from Harmsworth *et al.* 1990) and simulated magnetic and gravity responses. For each unit, the first number is bulk density; the second number is bulk susceptibility; the third number is NRM intensity, and its declination and inclination are given in brackets.

determine the magnetic and gravity responses over a mined, and hence well-known, iron-ore deposit in the basin.

The Section 6 deposit in the Tom Price mine (Figure 8) is located within an open east–west trending synform structure. The deposit is approximately 2 km long by 700 m wide, with a maximum ore depth of 160 m below surface (Harmsworth *et al.* 1990). High-grade hematite ore is confined almost entirely to the Dales Gorge Member, with only minor enrichment in the Joffre Member.

Calculated TMI and residual gravity anomalies over the Section 6 deposit are shown in Figure 8. As shown earlier, the *in situ* NRM carried by hematite ores in the Tom Price mine varies from site to site within a deposit, which implies that the *in situ* NRM of the orebody as a whole is likely to be scattered and thus can be neglected in the modelling. If no hematite enrichment occurred in BIFs, the model predicts TMI variations of close to 20 000 nT (dash-dot line). With highly magnetic BIFs being altered to less magnetic hematite ores, the amplitude of the TMI anomaly is reduced to a few thousand nano-Tesla (solid curve). A residual gravity anomaly of about +6.5 mGal, using the exposed Fortescue Group as the reference level, occurs over the deposit (dashed curve). Replacing the ore with BIF, a net anomaly of only +0.7 mGal occurs over the same location (dotted line).

DISCUSSION AND CONCLUSIONS

Our study reveals that a bimodal distribution of bulk susceptibility exists in the four major BIF formations in the Hamersley Basin. A BIF unit normally consists of a number of alternating BIF and shale members, and even within a BIF member, iron-rich bands alternate with chert-rich bands. For magnetic modelling, the bulk susceptibility of a BIF unit should be a volume-weighted average of the susceptibility of the alternating magnetite-rich and shale/chert-rich bands in the unit. For example, the Brockman Iron Formation contains shale members which account for about 20% of its whole volume, and some shale bands also exist in the BIF members (Thorne & Tyler 1997). As a result, it is reasonable to assign two-thirds of the average bulk susceptibility for fresh BIF as the mean bulk susceptibility for the whole formation for modelling purposes.

AMS also affects magnetic modelling involving BIF units. This, and previous studies (Jahren 1963; Clark & Schmidt 1986, 1994), show that BIF units have bedding-parallel or sub-bedding-parallel magnetic foliation with AMS of 1.5–4.0. This causes deflection of induced and remanent magnetisation directions towards the bedding. This results in changes in both the amplitude and geometry of the magnetic response. This effect is actually due to the layered nature of the BIF units, which is essentially the result of internal self-demagnetisation within the layers. If the effect of AMS is taken into account when the modelling then no separate self-demagnetisation correction for individual BIF units will be required. Otherwise, the effect of self-demagnetisation for BIF units will be doubly counted.

Our work confirms the presence of a regional magnetic overprint directed upward upwards the northwest, which is similar to findings of previous studies in the basin (Schmidt & Embleton, 1985; Clark & Schmidt 1986; Li *et al.* 1993). We note that there are at least 16 formations in the Mount Bruce Supergroup but previous studies were based on samples collected from only two formations in the Fortescue Group, namely the Mt Jope Volcanics (Schmidt & Embleton 1985) and the Jeerinah Formation (Li *et al.* 1993), and three formations in the Hamersley Group, namely the Brockman Iron and Weeli Wolli Formations (Clark & Schmidt 1986) and the Wittenoom Dolomite (Li *et al.* 1993). With the more extensive stratigraphic coverage in this study, our results not only reaffirm the presence of this northwesterly upward regional magnetic overprint in the Mount Bruce Supergroup, but also extend this overprint to as far as the Mount McGrath Formation in the Wyloo Group. The direction of this regional overprint is $\mathrm{Dec} = 310^{\circ}/\mathrm{Inc} = -27^{\circ}$. Magnetic modelling of the Hamersley Range demonstrates that the effect of this regional overprint has a significant influence on the magnetic responses in the region. Modelling conducted by Clark & Schmidt (1986, 1994) in the Turner Syncline, a more deformed area in the southern part of the basin, also demonstrated the importance of accounting for this NRM overprint for magnetic modelling in the basin.

ACKNOWLEDGEMENTS

The Minerals & Energy Research Institute of WA (MERIWA), BHP Iron Ore, Hamersley Iron Pty. Limited, and Robe River Iron Associates are thanked for partly supporting this research. Academic support and technical and field assistance, were provided especially by D. Kepert, M. Kneeshaw, J. Ronaszeki and T. Johnson (BHP), M. Pal, K. Dettbarn, J. Phillips and D. Flynn (HI), T. James, D. Mason and C. Robinson (RRIA), R. Hackney (UWA, now GA) and D. Martin (UWA) and R. Morris (CSIRO). WWG's PhD study was supported by an Overseas Postgraduate Research Scholarship of Commonwealth Government of Australia, and a UWA University Postgraduate Award. Geoscience Australia is thanked for giving permission to use the aeromagnetic image for supporting this research. We also appreciate constructive comments on the manuscript made by Drs Chris Klootwijk and Bob Musgrave. This is TIGeR publication #252.

REFERENCES

Butler R. F. 1992. *Paleomagnetism.* Blackwell Scientific Publications, Boston.

Butt A. L. & Flis M. F. 1997. The application of geophysics to iron ore mining in the Hamersley Basin, Western Australia. *Exploration Geophysics* **28**, 195–198.

Cawood P. A. & Tyler I. M. 2004. Assembling and reactivating the Proterozoic Capricorn Orogen: lithotectonic elements, orogenies, and significance. *Precambrian Research* **128**, 201–218.

Chamalaun F. H. & Dempsey C. E. 1978. *A survey of the magnetic properties of the banded iron formations, Hamersley Iron Basin, WA.* Publication **78/4**, Department of Earth Sciences, Flinders University.

Clark D. A. & Schmidt P. W. 1986. *Magnetic properties of the banded-iron formations of the Hamersley Group, WA.* CSIRO Division of Mineral Physics RIR 1638R (AMIRA Project 78/P96B: Applications of Rock Magnetism).

Clark D. A. & Schmidt P. W. 1994. Magnetic properties and magnetic signatures of BIFs of the Hamersley Basin and Yilgarn Block, Western Australia. *In*: Dentith M. C., Frankcombe K. F., Ho S. E., Shepherd J. M., Groves D. I. & Trench A. eds. *Geophysical signatures of Western Australian mineral deposits,* pp. 343–354. Geology and Geophysics Department (Key Centre) & UWA Extension, The University of Western Australia Publication No **26**.

Embleton B. J. J., Robertson W. A. & Schmidt P. W. 1979. *A survey of magnetic properties of some rocks from northwestern Australia.* CSIRO Division of Mineral Physics Investigations Report No. **129**.

Guo W. 1999. *Magnetic petrophysics and density investigations of the Hamersley Basin, Western Australia: implications for magnetic and gravity interpretation.* PhD thesis, The University of Western Australia.

Guo W. & Howard D. 2000. Interpretation of the crustal structure between the Hamersley and Ashburton Basins from gravity and magnetic data in the Wyloo area, Western Australia. *Exploration Geophysics* **31**, 33–38.

Guo W., Dentith M. C., Bird R. T. & Clark D. A. 2001. Systematic error analysis of demagnetisation and implications for magnetic interpretation. *Geophysics* **66**, 562–570.

Harmsworth R. A., Kneeshaw M., Morris R. C., Robinson C. J. & Shrivastava P. K. 1990. BIF-derived iron ores of the Hamersley Iron Basin. *In*: Hughes F. E. ed. *Geology of mineral deposits of Australia and Papua New Guinea,* pp. 617–642. Australasian Institute of Mining and Metallurgy.

Hawke P. J. & Flis M. F. 1997. Application of electrical techniques for iron ore exploration. *Exploration Geophysics* **28**, 242–246.

Jahren C. E., 1963. Magnetic susceptibility of bedded iron formation. *Geophysics* **28**, 756–766.

Kerr T. L., O'Sullivan A. P., Podmore D. C., Turner R. & Waters P. W. 1994. Geophysics and iron ore exploration: examples from the Jimblebar and Shay Gap-Yarrie regions, Western Australia. *In*: Dentith M. C., Frankcombe K. F., Ho S. E., Shepherd J. M., Groves D. I. & Trench A. eds. *Geophysical signatures of Western Australian mineral deposits,* pp. 355–367. Geology and Geophysics Department (Key Centre) & UWA Extension, The University of Western Australia Publication No **26**.

Kneeshaw M. 1984. Pilbara iron ore classification—a proposal for a common classification for BIF-derived supergene iron ore. In: *Proceedings of Australasian Institute of Mining and Metallurgy,* pp. 157–162. Australasian Institute of Mining and Metallurgy.

Li Z. X., Powell C. M. & Bowman R. 1993. Timing and genesis of Hamersley iron-ore deposits. *Exploration Geophysics* **24**, 631–636.

Li Z. X., Guo W. W. & Powell C. M. 2000. *The timing and genesis of the Hamersley iron ore deposits: a new palaeomagnetic approach.* Minerals and Energy Research Institute of Western Australia (MERIWA), Report **M242**.

Milligan P. R. & Franklin R. 2004. *Magnetic anomaly map of Australia, 4th edition, 1:15 000 000 scale*. Geoscience Australia, Canberra.

Morris R. C. 1985. Genesis of iron ore in banded iron-formation by supergene and supergene–metamorphic processes—a conceptual model. *In*: Wolf K. H. ed. *Handbook of strata-bound and stratiform ore deposits,* pp. 73–235. Elsevier, Amsterdam.

Porath H. & Chamalaun F. H. 1968. Palaeomagnetism of Australian haematite ore bodies II, Western Australia. *Geophysical Journal of the Royal Astronomical Society* **15**, 253–264.

Schmidt P. W. & Embleton B. J. J. 1985. Pre-folding and overprint magnetic signatures in Precambian (~2.9–2.7 Ga) igneous rocks from the Pilbara Craton and Hamersley Basin, NW Australia. *Journal of Geophysical Research* **90**, 2967–2984.

Schmidt P. W. & Clark D. A. 1994. Palaeomagnetism and magnetic anisotropy of Proterozoic banded-iron formations and iron ores of the Hamersley Basin, Western Australia. *Precambian Research* **69**, 133–155.

Seguin M. K. 1971. Discovery of direct-shipping iron ore by geophysical methods in the Central Part of the Labrador Trough. *Geophysical Prospecting* **19**, 950–960.

Tarling D. H. 1983. *Palaeomagnetism.* Chapman & Hall, London.

Thorne A. M., Tyler I. M., Blockley J. G. & Blight D. F. 1996. *Mount Bruce 1:250 000 map.* Western Australia Geological Survey, Perth.

Thorne A. M. & Tyler I. M. 1997. *Roy Hill 1:250 000 geological series explanatory notes, Western Australia.* Western Australia Geological Survey, Perth.

Trendall A. F. 1983. The Hamersley Basin. *In*: Trendall A. F. & Morris R. C. eds. *Iron-formation: facts and problems,* pp. 69–129. Elsevier, Amsterdam.

Trendall A. F., Compston W., Nelson D. R., De Laeter J. R. & Bennett V. C. 2004. SHRIMP zircon ages constraining the depositional chronology of the Hamersley Group, Western Australia. *Australian Journal of Earth Sciences* **51**, 621–644.

Webb J. E. 1966. The search for iron ore, Eyre Peninsula, South Australia. In: *SEG ed. Mining geophysics Vol. I: case histories,* pp. 379–390.SEG.

Received 26 August 2009; accepted 25 December 2010

APPENDIX 1: GENERAL AND DIRECTIONAL VECTOR ANALYSES

General vector analysis

To calculate the mean direction from a set of N vectors in Cartesian coordinates (x towards north, y towards east and z downwards, Figure 9), the three components X_i, Y_i and Z_i of individual vectors can be expressed by their direction cosines (l_i, m_i, n_i) and intensity (J_{ri}) as

$$\begin{aligned} X_i &= J_{ri} l_i = J_{ri} \cos I_i \cos D_i \\ Y_i &= J_{ri} m_i = J_{ri} \cos I_i \sin D_i \quad (i = 1, 2, \ldots, N) \\ Z_i &= J_{ri} n_i = J_{ri} \sin I_i \end{aligned} \tag{1}$$

where D_i and I_i are the declination with respect to north and inclination with respect to horizontal of the ith vector, respectively. The three components (X, Y, Z) of the mean vector are given by

$$\begin{aligned} X &= \frac{\sum_{i=1}^{N} X_i}{N} \\ Y &= \frac{\sum_{i=1}^{N} Y_i}{N} \\ Z &= \frac{\sum_{i=1}^{N} Z_i}{N} \end{aligned} \tag{2}$$

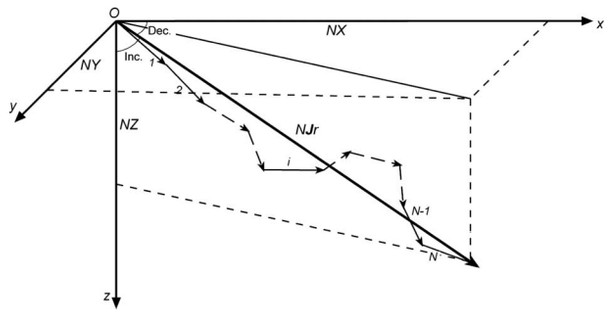

Figure 9 Resultant of N vectors for the general vector analysis (GVA). (x towards north, y towards east and z downwards, $\boldsymbol{J_r}$, the mean vector of NRMs).

The intensity (J_r) of the mean vector $\boldsymbol{J_r}$ is determined through

$$J_r^2 = X^2 + Y^2 + Z^2 \tag{3}$$

The declination and inclination of the mean direction can be derived from Equations 2 and 3 as

$$D = \tan^{-1}\left(\frac{Y}{X}\right) \quad \text{and} \quad I = \sin^{-1}\left(\frac{Z}{J_r}\right) \tag{4}$$

The standard deviations of the three components (σ_x, σ_y, σ_z) are given by

$$\sigma_j = \sqrt{\frac{\sum_{i=1}^{N}\left(j_i - \bar{j}\right)^2}{N-1}} \quad (j = X, Y, Z) \tag{5}$$

where $\bar{j}$ is the mean of one of the three components and given by

$$\bar{j} = \frac{1}{N}\sum_{i=1}^{N} j_i \tag{6}$$

A unified standard deviation (σ_r) of this mean vector can be determined by

$$\sigma_r = \frac{1}{J_r}\sqrt{(X\sigma_x)^2 + (Y\sigma_y)^2 + (Z\sigma_z)^2} \tag{7}$$

To estimate the precision of the mean and the extent of scatter of a set of vectors, we define an angular deviation (λ) of the mean shown in Figure 10 as

$$\lambda = \tan^{-1}\left(\frac{\sigma_r}{J_r}\right) \tag{8}$$

The mean vector is determined by its declination (D) and inclination (I), both possibly varying from $-\lambda$ to $+\lambda$, and by its intensity (J_r) varying from $J_r(1 - \tan\lambda)$ to $J_r(1 + \tan\lambda)$.

Due to the unevenness of individual NRM vectors in GVA, it is difficult to set up an absolute measure similar to α_{95} in Fisher analysis to quantify the extent of scatter of a set of vectors for GVA. However, magnetic simulation showed that a magnetic anomaly may largely keep the same pattern if an angular deviation is within 22.5° (Guo 1999). Therefore, in this study, a mean of a set of vectors with $\lambda < 22.5°$ is regarded as concentrated whereas that with λ between 22.5° and 30° is regarded as marginally concentrated.

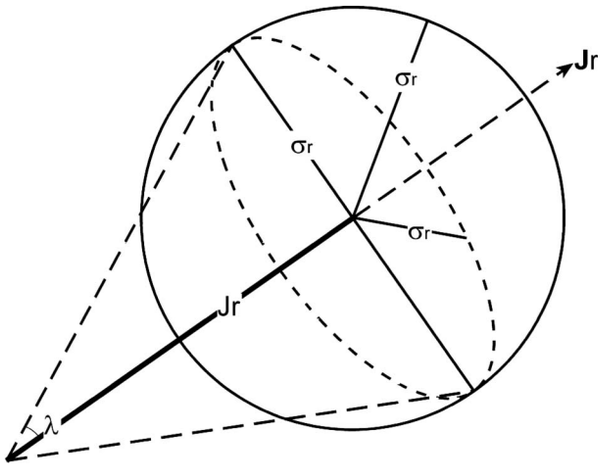

Figure 10 Relationships among the parameters of the general vector analysis (GVA).

Directional vector analysis (DVA)

In some cases, such as a magnetically homogeneous geological unit or a weakly magnetised geological body, NRM direction becomes the major concern in statistical analysis. In such cases, each NRM is regarded as a unit vector.

The direction cosines (l, m, n) of the mean direction, calculated through the direction cosines (l_i, m_i, n_i) of a set of N unit vectors, are given by

$$l = \frac{\sum_{i=1}^{N} l_i}{R}$$

$$m = \frac{\sum_{i=1}^{N} m_i}{R} \tag{9}$$

$$n = \frac{\sum_{i=1}^{N} n_i}{R}$$

where $\boldsymbol{R}$ is the resultant vector with length R given by

$$R = \sqrt{\left(\sum_{i=1}^{N} l_i\right)^2 + \left(\sum_{i=1}^{N} m_i\right)^2 + \left(\sum_{i=1}^{N} n_i\right)^2} \tag{10}$$

The relationship of $\boldsymbol{R}$ to the N individual unit vectors is shown in Figure 11. The declination (D) and inclination (I) of the mean direction can be derived from Equations 9 and 10 as

$$D = \tan^{-1}\left(\frac{m}{l}\right) \quad \text{and} \quad I = \sin^{-1} n \tag{11}$$

The angular deviation, δ, is termed as

$$\delta = \cos^{-1}\left(\frac{R}{N}\right) \tag{12}$$

This angular deviation is similar to that proposed in Fisher analysis (Tarling 1983; Butler 1992), and the mean

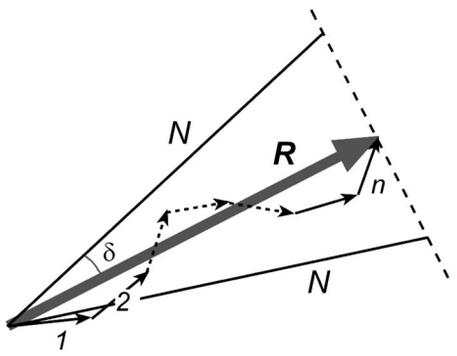

Figure 11 Relationships among parameters of the directional vector analysis (DVA).

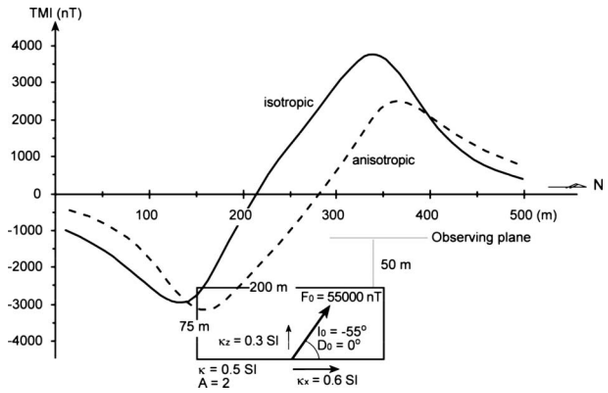

Figure 12 TMI responses to isotropic (solid line) and anisotropic (dashed line) induced magnetisation over a 2D horizontal rectangular object. Profile is perpendicular to the strike of the rectangular object and parallel to the Earth's magnetic field (EMF). F_0, total intensity of the EMF; I_0, inclination of the EMF; D_0, declination of the EMF; κ, bulk susceptibility; κ_x, bedding-parallel susceptibility; κ_z, bedding-perpendicular susceptibility; $A = \kappa_x/\kappa_z$, anisotropy of magnetic susceptibility.

direction from DVA is also exactly the same as the Fisher mean. However, it should be noted that DVA is generally applicable to any directional data sets, but theoretically, the Fisher analysis is for data sets with a spherical normal distribution only.

Analogous to GVA, a mean of a set of unit vectors with an angular deviation δ of $<22.5^\circ$ is regarded concentrated, whereas that with δ between 22.5° and 30° is regarded marginally concentrated. GVA and DVA generally give different mean directions for the same data set, but the difference should be small if the studied geological unit is magnetically homogeneous.

APPENDIX 2: IMPLICATIONS OF AMS, NRM AND SELF-DEMAGNETISATION FOR MAGNETIC MODELLING

Anisotropy of magnetic susceptibility (AMS)

This and previous studies (Jahren 1963; Clark & Schmidt 1986, 1994) show that BIF units normally have bedding-parallel or sub-bedding-parallel magnetic foliation with AMS of 1.5–4.0. In the following discussion, zero NRM intensity is assumed so as to highlight the effect of AMS.

Figure 12 shows the total magnetic intensity (TMI) profile over a 2D horizontal rectangular object with strike perpendicular to the Earth's Magnetic Field (EMF) and the profile. The solid curve represents the TMI response over this model with an isotropic susceptibility of 0.5 SI. Assuming the presence of an AMS of 2.0 for this model, a bulk susceptibility of 0.5 SI will be decomposed to a horizontal susceptibility of 0.6 SI and a vertical susceptibility of 0.3 SI due to anisotropy. The dashed curve shows the TMI response of the same model with an AMS of 2.0. In this case, anisotropy makes the TMI 'compressed' in both shape and magnitude, and the extreme positions shifted, compared with that of isotropy in magnetic susceptibility.

Assuming a model of a 2D horizontal sheet (Figure 13), its induced magnetisation (J_i) and inclination (I_i), without considering the AMS effect, are given by:

$$J_i = \kappa F_0 \quad \text{and} \quad I_i = I_0 \tag{13}$$

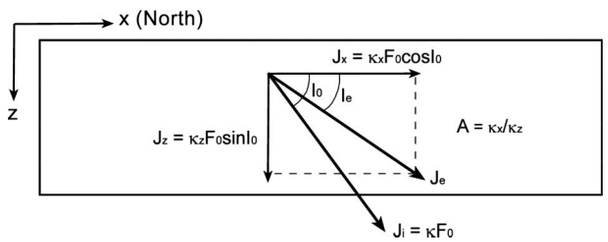

Figure 13 Schematic model showing AMS effect on induced magnetisation. $\mathbf{J}_i$, induced magnetisation; $\mathbf{J}_e$, effective magnetisation; I_e, inclination of effective magnetisation; $\mathbf{J}_x$, bedding-parallel component of induced magnetisation; $\mathbf{J}_z$, bedding-perpendicular component of induced magnetisation; meanings of other parameters being the same as those in Figure 12.

where κ is the bulk susceptibility, F_0 is the total intensity of the EMF, and I_0 is the inclination of the EMF.

When AMS is considered, the bedding-parallel (along x) and bedding-perpendicular (along z) components of induced magnetisation are given by

$$J_x = \kappa_x F_0 \cos I_0 \quad \text{and} \quad J_z = \kappa_z F_0 \sin I_0 \tag{14}$$

where κ_x and κ_z are bedding-parallel and bedding-perpendicular susceptibilities with $A = \kappa_x/\kappa_z$. Since BIF units have a bedding-parallel magnetic foliation, the maximum and intermediate components of susceptibility on this magnetic foliation should be the same, i.e. $\kappa_1 = \kappa_2 = \kappa_x$. Hence

$$\kappa = \frac{\kappa_1 + \kappa_2 + \kappa_3}{3} = \frac{2\kappa_x + \kappa_z}{3} = \frac{(2A+1)\kappa_z}{3} \tag{15}$$

The corresponding effective magnetisation (J_e) and inclination (I_e) after considering AMS can then be expressed as

$$J_e = \sqrt{J_x^2 + J_z^2} = \kappa_z F_0 \sqrt{\sin^2 I_0 + A^2 \cos^2 I_0} \tag{16}$$

and

$$I_e = \tan^{-1}\left(\frac{J_z}{J_x}\right) = \tan^{-1}\left(\frac{1}{A}\tan I_0\right) \quad (17)$$

Thus, the differences in magnetisation intensity ($\Delta J = J_i - J_e$) and in inclination ($\Delta I = I_i - I_e$) with and without consideration of AMS effects can be determined from Equations 13–17. The relative difference (error) of magnetisation intensity (δJ) is given as

$$\delta J = \frac{\Delta J}{J_i} = \left(1 - \frac{3}{2A+1}\sqrt{\sin^2 I_0 + A^2\cos^2 I_0}\right) \quad (18)$$

and the inclination difference is given by

$$\Delta I = I_i - I_e = I_0 - \tan^{-1}\left(\frac{1}{A}\tan I_0\right) \quad (19)$$

The differences are dependent not only on AMS, but also on the inclination of the EMF. Figure 14 presents the relative difference in magnetisation intensity *vs* AMS with various inclinations of the EMF. In the region where inclination of the EMF is around 45°, the relative difference is always less than 5% for AMS ranging from 1 to 10, so the effect of AMS on intensity of induced magnetisation, and accordingly on the amplitude of a magnetic anomaly produced by induced magnetism only, is insignificant. The inclination of the EMF in the Hamersley Basin is about –55° (Milligan & Franklin 2004), so the corresponding relative difference in induced magnetisation in the basin, with an AMS of ~2, is about 15% less than that without considering anisotropy, which is shown in Figure 12.

Figure 15 presents the difference in magnetic inclination *vs* AMS with various inclinations of the EMF. Inclination difference increases with increasing AMS as the induced magnetisation approaches the bedding of a sheet-like body. This means that the horizontal positions of characteristic points in the magnetic profile, with and without the AMS effect, will

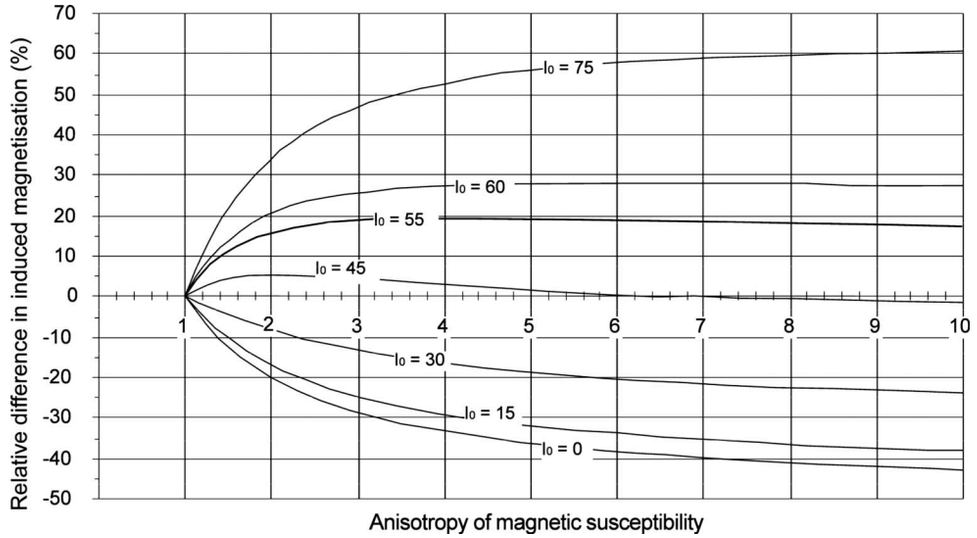

Figure 14 Relative intensity differences in induced magnetisation versus AMS.

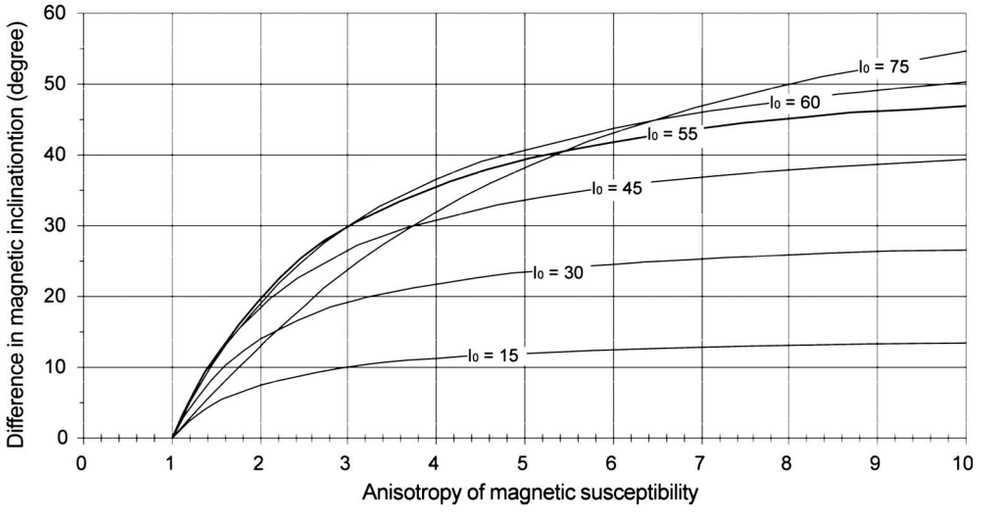

Figure 15 Deflection of magnetic inclination versus AMS.

be offset from each other, which is also demonstrated in Figure 12.

The bedding-parallel AMS of BIFs also makes the remanent magnetisation carried by BIFs deflect towards the bedding, which has been analysed in detail by Schmidt & Clark (1994).

Natural remanent magnetisation (NRM)

Detailed analysis of pre-folding and post-folding NRM on magnetic modelling has been discussed by Clark & Schmidt (1986, 1994). Here we only use a simple example to illustrate the influence of this effect. Figure 16 shows the magnetic responses of both pre-folding NRM and post-folding NRM over a synthetic syncline model. In this case, compared with the magnetic response of pre-folding NRM, post-folding NRM changes not only the shape of the curve, but also the horizontal localities of extreme values. As a result, NRM must be taken into account in magnetic data interpretation, unless either the induced magnetisation is far stronger than NRM or NRM is scattered in direction.

Self-demagnetisation

In the case of weak to intermediate magnetism ($\kappa < 0.1$ SI), the effect of self-demagnetisation is insignificant and can be neglected in magnetic modelling. However, such an effect is important when the magnetic body has a high susceptibility and/or remanence. Detailed analysis regarding the effect of self-demagnetisation can be found in Guo *et al.* (2001). For BIF units, if AMS effect has been taken into account during modelling, there is no need to conduct self-demagnetisation correction separately. This is because the AMS effect of BIF units to magnetic modelling is actually due to the layered texture of BIF units, which is essentially the result of internal self-demagnetisation within the BIF units.

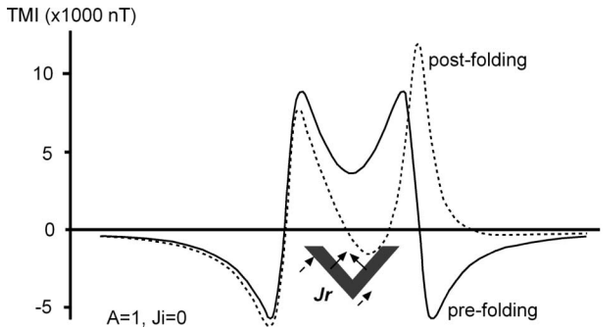

Figure 16 TMI responses over a synthetic syncline with pre-folding NRM (solid line) and post-folding NRM (dashed line).